Corrosion Science 138 (2018) 20–27

Contents lists available at ScienceDirect

Corrosion Science

journal homepage: www.elsevier.com/locate/corsci

Effects of Cr addition on thermal stability, soft magnetic properties and corrosion resistance of FeSiB amorphous alloys

D.D. Xu[a,b,1], B.L. Zhou[a,b,1], Q.Q. Wang[a,b], J. Zhou[a,b], W.M. Yang[c], C.C. Yuan[a,b], L. Xue[a,b], X.D. Fan[a,b], L.Q. Ma[d], B.L. Shen[a,b,c,*]

[a] School of Materials Science and Engineering, Southeast University, Nanjing 211189, China
[b] Jiangsu Key Laboratory for Advanced Metallic Materials, Nanjing, 211189, China
[c] Institute of Massive Amorphous Metal Science, China University of Mining and Technology, Xuzhou, 221116, China
[d] School of Materials Science and Engineering, Nanjing Tech University, Nanjing 211189, China

ARTICLE INFO

Keywords:
A. Amorphous alloy
B. Polarization
B. XPS
C. High corrosion resistance
C. Passive films

ABSTRACT

The effects of Cr addition on the thermal stability, soft magnetic properties and corrosion resistance of $Fe_{79.5-x}Si_{9.5}B_{11}Cr_x$ amorphous alloys were detailed investigated. It was found that Cr addition has multiple effects on improving those properties of FeSiB amorphous alloys. As Cr content increases from 0 to 5 at%, the coercive force decreases from 2.46 to 2.02 A/m, and the corrosion rate of the alloys in 0.1 M NaCl solution also decreases from 1.83×10^{-1} to 3.91×10^{-4} mm·year^{-1}. Besides, the passive region exceeds 1.13 V for the alloy containing 7 at% of Cr.

1. Introduction

FeSiB amorphous alloys with good soft magnetic properties of high saturation magnetizations and low core losses have been commercially produced and widely applied as magnetic cores of distribution transformers in power grid [1,2]. However, atmospheric and pitting corrosions are inevitable for FeSiB amorphous alloys when they are used as cores of distribution transformers and electronic component parts in air, especially in salted environment near sea. Therefore, it is important for applications of FeSiB amorphous alloys to enhance their corrosion resistance. Although the corrosion behavior of FeSiB amorphous alloys has been studied in earlier research [3–6], there is little study of the effect of compositional optimization on the corrosion resistance of FeSiB amorphous alloys. It has been verified that Cr addition is effective to improve the corrosion resistance of Fe-based amorphous alloys [7–10], such as FeCrMoCB bulk glassy alloys in HCl solutions [8,11]. In addition, Shen et al. found that the substitution of a small amount of Fe with Cr can increase the glass-forming ability as well as the corrosion resistance of FeMoGaPCBSi bulk glassy alloys in NaCl solutions [12]. Moreover, it was also found in the early 1980s that Cr addition can improve the soft magnetic properties of the FeSiB amorphous alloys, which not only decreases the coercive force and magnetic core loss, but also increases the initial permeability [13]. Therefore, it is reasonable to develop FeSiB amorphous alloys with high corrosion resistance, combined with high thermal stability and good soft magnetic properties by substituting a small amount of Fe with Cr, to meet the multiple needs of applications of FeSiB amorphous alloys used as magnetic cores of transformers and electronic components in severe environments.

In this paper, with the aim of developing FeSiB amorphous alloys with good multiple properties, such as high corrosion resistance and low core loss, $Fe_{79.5-x}Si_{9.5}B_{11}Cr_x$ (x = 0, 1, 2, 3, 4, 5, 7, 9 and 11 at%) amorphous alloys were prepared, and the thermal stability, corrosion behavior and soft magnetic properties of the alloys were carefully measured. The origin for the effect of Cr addition on those properties of FeSiB amorphous alloys was investigated and discussed in detailed. This study will be beneficial to explore a new FeSiB amorphous alloy system with high corrosion resistance and thermal stability as well as excellent soft magnetic properties.

2. Experimental procedure

Multi-component $Fe_{79.5-x}Si_{9.5}B_{11}Cr_x$ (x = 0, 1, 2, 3, 4, 5, 7, 9 and 11 at%) ingots were prepared by arc melting the mixtures of high purity Fe (99.99 wt%), Si (99.999 wt%), B (99.5 wt%) and Cr (99.95 wt%) in Ti-gettered argon atmosphere. Ribbons with a width of 1.5 mm and thickness of 30 μm were prepared by single-roller melt spinning method. The amorphous structure and thermal properties of the ribbons were investigated by X-ray diffraction (XRD) with Cu *K*α radiation and

* Corresponding author at: School of Materials Science and Engineering, Southeast University, Nanjing 211189, China.
E-mail address: blshen@seu.edu.cn (B.L. Shen).
[1] Authors contributed equally to this work.

https://doi.org/10.1016/j.corsci.2018.04.006
Received 23 October 2017; Received in revised form 31 March 2018; Accepted 2 April 2018
Available online 07 April 2018
0010-938X/

differential scanning calorimetry (DSC) at a heating rate of 0.33 K/s, respectively. The isothermal annealing treatment at different temperature was performed in a vacuum atmosphere followed by water quenching. The saturation magnetization (I_s) and coercive force (H_c) were measured with a vibrating sample magnetometer (VSM) under an applied field of 800 kA/m and a B–H loop tracer under a field of 1 kA/m, respectively. Prior to measurement of H_c, ribbons were annealed at 110 K below the onset crystallization temperature of the first peak (T_{x1}) for 600 s to remove internal stress caused by rapid quenching process.

The corrosion behaviors were investigated by immersion tests and electrochemical measurements. Prior to the immersion and electrochemical tests, the ribbons were washed with alcohol by ultrasonic cleaning for 180 s and dried in air. The corrosion rates were estimated from the weight loss of the ribbons after immersed in 0.1 M NaCl solution for 120 h at room temperature. The electrochemical measurement was conducted in a three-electrode cell using a platinum counter electrode and a Ag/AgCl reference electrode. Potentiodynamic polarization curves were measured by an electrochemical work station with a potential sweep rate of 4 mv/s in 0.1 M NaCl solution when the open-circuit potential had been stabilized after immersing the specimens in the solution within 1 h. After immersion measurements, the surface morphology of the ribbons was observed by scanning electron microscopy (SEM), and the bonding states of the sample surface were evaluated by X-ray photoelectron spectroscopy (XPS) using a Kratos AXIS ULTRA^{DLD} instrument with a monochromic Al K_α X-ray source ($h\nu$ = 1486.6 eV). The power was 120 W and the X-ray spot size was set as 700 × 300 μm. The pass energy of the XPS analyzer was set at 20 eV, and the base pressure of the analysis chamber was lower than 5×10^{-9} Torr. The compositions of the surface film and the underlying alloy surface were quantitatively determined with a previously proposed method using the integrated intensities of photoelectrons under the assumption of a three-layer model of (1) an outermost contaminant hydrocarbon layer of uniform thickness, (2) a surface film of uniform thickness and (3) an underlying alloy surface of infinite thickness [14,15]. All spectra were calibrated using the binding energy (BE) of C 1*s* (284.8 eV) as a reference [16,17].

3. Results and discussion

3.1. Thermal and magnetic properties of $Fe_{79.5-x}Si_{9.5}B_{11}Cr_x$ amorphous alloys

Fig. 1 shows DSC curves of the $Fe_{79.5-x}Si_{9.5}B_{11}Cr_x$ amorphous ribbons. No obvious glass transition was observed in any of the DSC curve, which was consistent with the previous results [18]. With increasing Cr

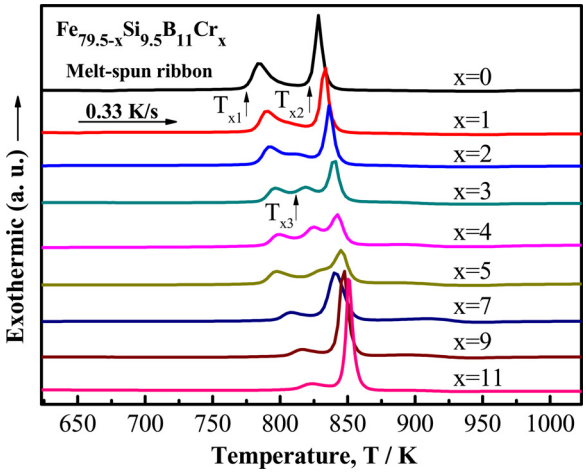

Fig. 1. DSC curves of the $Fe_{79.5-x}Si_{9.5}B_{11}Cr_x$ (x = 0, 1, 2, 3, 4, 5, 7, 9 and 11 at %) amorphous ribbons at a heating rate of 0.33 K/s.

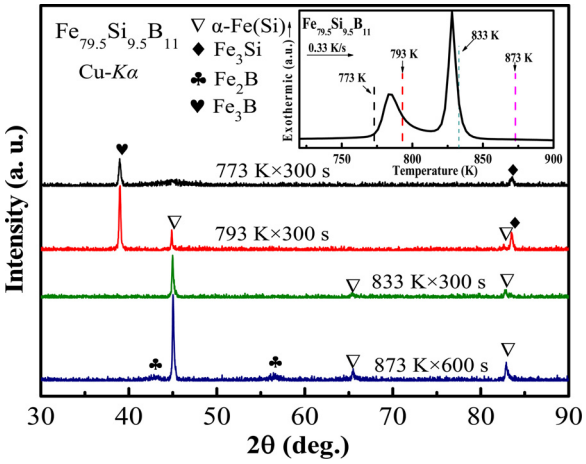

Fig. 2. XRD patterns of $Fe_{79.5}Si_{9.5}B_{11}$ amorphous ribbons annealed at different temperatures. The insert shows DSC curve of $Fe_{79.5}Si_{9.5}B_{11}$ amorphous ribbons. The dash lines in the insert display the annealed temperatures.

content, T_{x1} gradually shifts towards high temperature side, while the crystallization behavior changes from two-stage to three-stage, and then changes to two-stage crystallization again, accompanying a rise of the onset crystallization temperature of the second crystallization stage (T_{x2}). To explore the origin of crystallization, the crystallization behaviors were investigated by annealing three representative alloys at different annealing conditions, including $Fe_{79.5}Si_{9.5}B_{11}$, $Fe_{76.5}Si_{9.5}B_{11}Cr_3$ and $Fe_{68.5}Si_{9.5}B_{11}Cr_{11}$ amorphous ribbons. Figs. 2–4 show the XRD patterns of these three amorphous ribbons after annealed at different temperature and time. As shown in Fig. 2, the XRD patterns of the $Fe_{79.5}Si_{9.5}B_{11}$ amorphous ribbon subjected to annealing for 300 s at 773 and 793 K, corresponding to the temperatures just below and above the first exothermic peak in the DSC curve (shown in insert in Fig. 2), are identified as mixed Fe_3B, Fe_3Si phases, and mixed Fe_3B, Fe_3Si, α-Fe(Si) phases, respectively. The XRD pattern of the sample subjected to annealing for 300 s at 833 K corresponding to the temperature just above the second exothermic peak are identified as a single α-Fe(Si) phase. It is interesting to see from the XRD patterns of those precipitation phases that the intensity of the peaks of both Fe_3B and Fe_3Si phases increased largely as annealing temperature increased from 773 to 793 K, but disappeared suddenly and completely as annealing temperature increased from 793 to 833 K. However, the peaks of α-Fe(Si) phase didn't appear until the annealing temperature reached

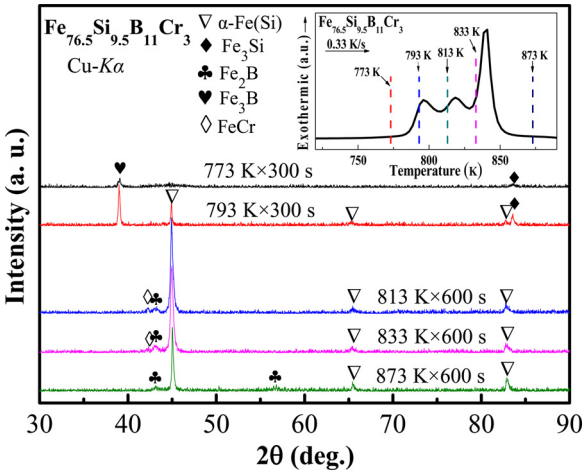

Fig. 3. XRD patterns of $Fe_{76.5}Si_{9.5}B_{11}Cr_3$ amorphous ribbons annealed at different temperatures. The insert shows DSC curve of $Fe_{76.5}Si_{9.5}B_{11}Cr_3$ amorphous ribbons. The dash lines in the insert display the annealed temperatures.

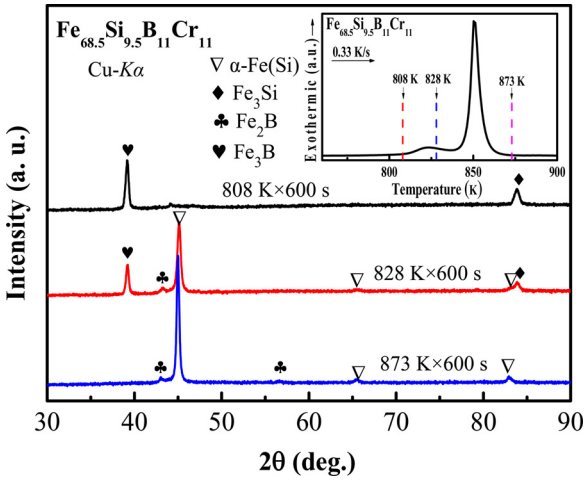

Fig. 4. XRD patterns of $Fe_{68.5}Si_{9.5}B_{11}Cr_{11}$ amorphous ribbons annealed at different temperatures. The insert shows DSC curve of $Fe_{68.5}Si_{9.5}B_{11}Cr_{11}$ amorphous ribbons. The dash lines in the insert display the annealed temperatures.

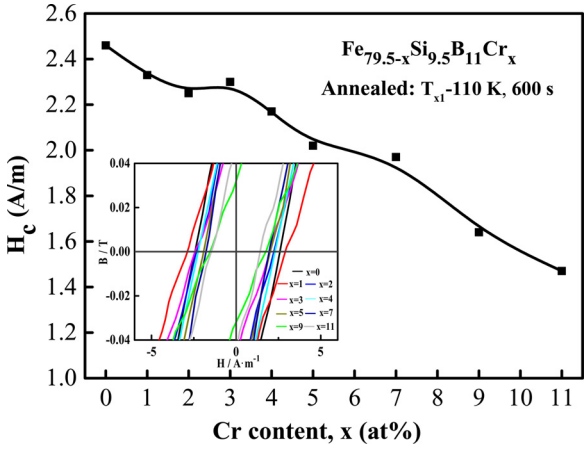

Fig. 5. Cr content dependences of the coercivity (H_c) for the $Fe_{79.5-x}Si_{9.5}B_{11}Cr_x$ (x = 0, 1, 2, 3, 4, 5, 7, 9 and 11 at%) amorphous ribbons. Hysteresis B–H loops of $Fe_{79.5-x}Si_{9.5}B_{11}Cr_x$ amorphous ribbons are displayed in the insert.

793 K, and increased gradually as the annealing temperature increased to 833 K, then increased largely with increasing the annealing temperature to 873 K. Therefore, it is considered that the first exothermic peak can be attributed to the precipitation of Fe_3B and Fe_3Si phases, while the second exothermic peak can be attributed to the precipitation of α-Fe(Si) phase. As the two exothermic peaks locate close to each other, a certain amount of precipitation of α-Fe(Si) phase in the alloy annealed at 793 K for 300 s is reasonable to be detected. For $Fe_{76.5}Si_{9.5}B_{11}Cr_3$ amorphous alloy, the crystallization is a three-stage behavior with a third exothermic peak between the first and second exothermic peak in DSC curve, as shown in Fig. 1 and the insert in Fig. 3. The onset crystallization temperature of the third peak is noted as T_{x3}. It is seen from the XRD patterns that the precipitation phases corresponding to the first and second exothermic peaks are the same with those of the $Fe_{79.5}Si_{9.5}B_{11}$ amorphous alloy, while the precipitation phase corresponding to the third exothermic peak is confirmed as FeCr phase. With further increasing Cr content, as shown in the insert in Fig. 4, the crystallization behavior changed back to two-stage crystallization stage, and the precipitation phases are the same with those of the $Fe_{79.5}Si_{9.5}B_{11}$ amorphous alloy. It is interesting that the precipitation phases for all the samples annealed at 873 K for 600 s are mixed α-Fe(Si) and Fe_2B phases, without appearance of FeCr phase. In addition, the XRD patterns of the Fe_3B and Fe_3Si phases for $Fe_{76.5}Si_{9.5}B_{11}Cr_3$ amorphous alloy are much weaker than those of $Fe_{79.5}Si_{9.5}B_{11}$ amorphous alloy annealed at the same condition of 773 K for 300 s, also suggesting the better thermal stability of $Fe_{76.5}Si_{9.5}B_{11}Cr_3$ compared to $Fe_{79.5}Si_{9.5}B_{11}$ amorphous alloy. Therefore, it is reasonable to conclude that the thermal stability of the $Fe_{79.5}Si_{9.5}B_{11}$ amorphous alloy can be increased with a small amount of Cr addition.

The influence of Cr addition on the magnetic properties of FeSiB amorphous alloys were measured detailed, and the data are summarized in Table 1. The I_s of the alloys decreased from 1.63 to 0.65 T as Cr content increased from 0 to 11 at%, because of the substitution of Fe with non-ferromagnetic element Cr. Besides, it is interesting to see that H_c also monotonously decreased from 2.46 to 1.47 A/m as shown in Fig. 5, with the insert in the figure showing the part of hysteresis loops with different Cr content. Therefore, it can be concluded that the soft magnetic properties of the FeSiB amorphous alloys were significantly improved with increasing Cr content although the I_s was decreased. It has been reported that the origin of low coercivity of Fe-based glassy alloy is the low number density of domain wall pinning sites, which are the agglomeration of vacancy-type point defects resulting from free volume in the amorphous/glassy alloy [19,20]. As mentioned former, the thermal stability of the FeSiBCr amorphous alloy increases with increasing Cr content, indicating the reduced density of defects in the alloys. As a result, the decreased coercivity of this amorphous alloy with increasing Cr content can be attributed to the improvement of thermal stability with Cr addition, which is consistent with the previous results [12].

3.2. Corrosion behavior of $Fe_{79.5-x}Si_{9.5}B_{11}Cr_x$ amorphous alloys

Fig. 6 shows the average corrosion rates of $Fe_{79.5-x}Si_{9.5}B_{11}Cr_x$ amorphous ribbons immersed in 0.1 M NaCl solution open to air at room temperature for 120 h. The corrosion rate decreases gradually from 1.83×10^{-1} to 1.17×10^{-1} mm·year^{-1} with Cr addition increasing from 0 to 4 at%. As Cr content further increases from 4 to 5 at %, the corrosion rate decreases rapidly from 1.17×10^{-1} to 3.91×10^{-4} mm·year^{-1}. However, when Cr content continuously increases to 11 at%, no significant change is observed for the corrosion rate, which maintains around 3.91×10^{-4} mm·year^{-1}. It is noted that the corrosion rate for the alloy with composition of 5 at% Cr is three orders of magnitude lower than that of the 4 at% Cr containing alloy. These results reveal that the corrosion resistance of the FeSiB amorphous alloys is effectively enhanced by a small amount of Cr addition.

The SEM micrographs of wheel surfaces of the $Fe_{79.5-x}Si_{9.5}B_{11}Cr_x$ amorphous ribbons with Cr addition of 0, 3, 4, and 5 at% after the immersion test in 0.1 M NaCl solution are shown in Fig. 7. The surface of the Cr-free alloy was badly damaged as shown in Fig. 7(a). The oxidation layer (marked as A_f) confirmed by EDX analysis due to its high oxygen content of 34.92 at% as shown in Table 2 peeled off heavily from matrix, resulting in the further erosion of the exposed matrix (marked as A_m) by NaCl solution. With increasing Cr addition, the damage of the alloy surface was largely reduced. When Cr addition increased to 3 at%, the surface layer did not peel off from the alloy

Table 1
The magnetic properties of the $Fe_{79.5-x}Si_{9.5}B_{11}Cr_x$ (x = 0, 1, 2, 3, 4, 5, 7, 9 and 11 at%) amorphous ribbons.

$Fe_{79.5-x}Si_{9.5}B_{11}Cr_x$	x = 0	x = 1	x = 2	x = 3	x = 4	x = 5	x = 7	x = 9	x = 11
I_s (T)	1.63	1.56	1.44	1.35	1.27	1.19	1.01	0.83	0.65
H_c (A/m)	2.46	2.33	2.25	2.30	2.17	2.02	1.97	1.64	1.47

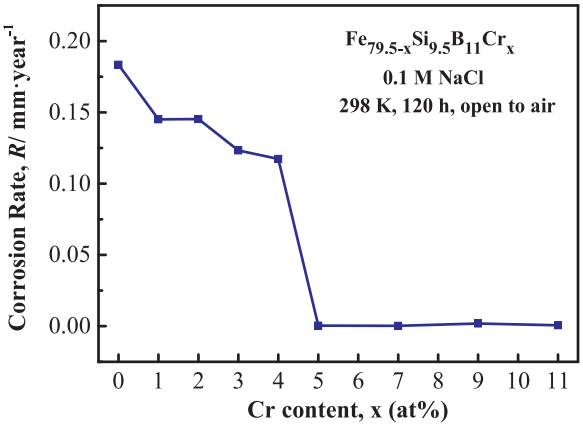

Fig. 6. Corrosion rates of the as-spun $Fe_{79.5-x}Si_{9.5}B_{11}Cr_x$ ($0 \le x \le 11$) amorphous ribbons in 0.1 M NaCl solution at room temperature.

matrix, with only some cracks and particles (marked as P) appearing on the surface, as shown in Fig. 7(b), the oxygen content of this oxidation layer decreased to 8.76 at%. As shown in Figs. 7(c) and (d), with further increasing Cr content to 4 and 5 at%, the oxidation layers densely covered on the surfaces and no crack was found, though some particles remained on the surface of the 4 at% Cr-containing alloy. It should be noted here that no particle or crack can be found on the surface of the 5 at% Cr-containing alloy, indicating the alloy exhibits excellent corrosion resistance, which is consistent with the rapid decrease of the corrosion rate for the 5 at% Cr-containing alloy as shown in Fig. 6. The high corrosion resistance of the alloy with 5 at% Cr can be attributed to the formation of a homogeneous passive film covering on the alloy surface. The surface morphology of the FeSiBCr alloys with 7–11 at% Cr addition after immersion tests are the same with 5 at% Cr-containing

Table 2
The elemental analysis on the surface of the amorphous $Fe_{79.5-x}Si_{9.5}B_{11}Cr_x$ (x = 0, 3 at%) ribbons in the wheel surfaces after immersion test by EDX.

Alloy	Position	Fe (at%)	Si (at%)	Cr (at%)	O (at%)
x = 0	A_m	48.13	4.6	–	4.96
	A_f	30.86	5.15	–	34.92
	P	24.81	3.3	–	23.4
x = 3	A_m	80.02	12.29	3.21	2.06
	A_f	60.86	20.47	5.56	8.76
	P	57.91	10.99	1.41	20.22

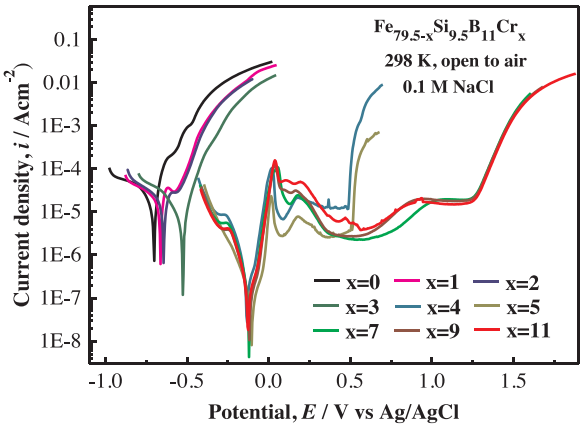

Fig. 8. Potentiodynamic polarization curves of $Fe_{79.5-x}Si_{9.5}B_{11}Cr_x$ (x = 0, 1, 2, 3, 4, 5, 7, 9 and 11 at%) amorphous ribbons in 0.1 M NaCl solution at room temperature.

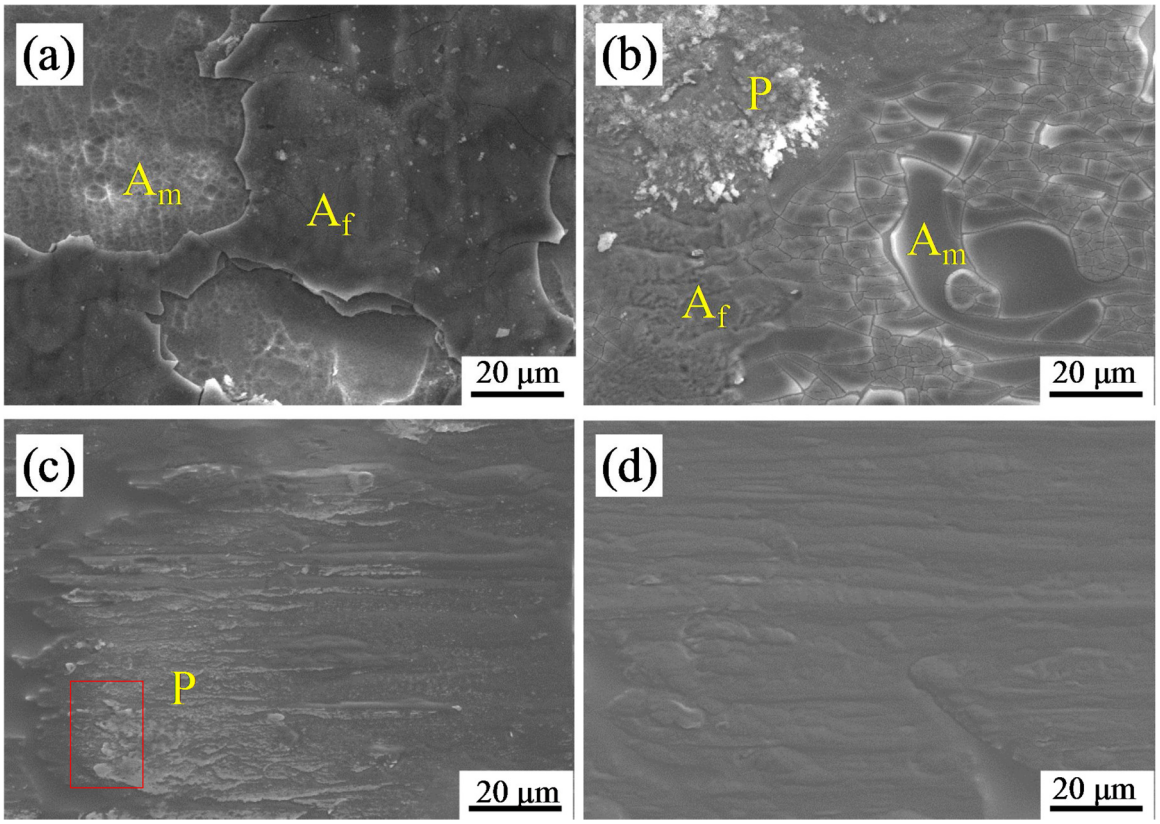

Fig. 7. SEM micrographs of the surface of $Fe_{79.5-x}Si_{9.5}B_{11}Cr_x$ amorphous ribbons after immersing in 0.1 M NaCl solution for 120 h at room temperature. ((a) x = 0; (b) x = 3; (c) x = 4; (d) x = 5; A_m: the matrix area; A_f: the oxidation films; P: the particles).

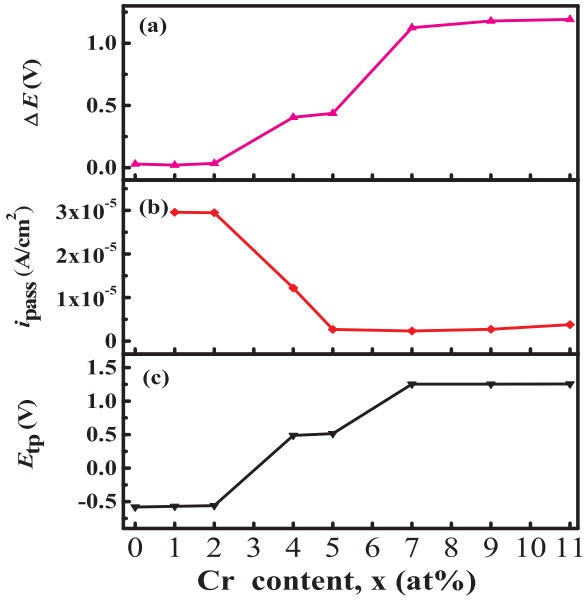

Fig. 9. Characteristic parameters obtained from Fig. 8: (a) passive potential region (ΔE), (b) passive current density (i_{pass}), (c) transpassive potential (ΔE_{tp}).

FeSiBCr alloy (data not shown).

To further evaluate the corrosion behavior of $Fe_{79.5-x}Si_{9.5}B_{11}Cr_x$ amorphous alloys, the potentiodynamic polarization measurement was systematically performed. Fig. 8 shows the polarization curves of the as-spun $Fe_{79.5-x}Si_{9.5}B_{11}Cr_x$ ribbons measured in 0.1 M NaCl solution which opens to air at room temperature. It is seen that the Cr-free alloy suffers from corrosion by a slight anodic polarization without passive region. However, except for the alloy with 3 at% Cr, all the other alloys containing a small amount of Cr show obvious passivation in their anodic polarization curves. With more Cr addition (> 3 at%), the alloys passivated with wide passive regions (ΔE), low passive current density (i_{pass}) and low transpassive potential (E_{tp}). Characteristic parameters, including ΔE, i_{pass} and E_{tp}, obtained from the potentiodynamic polarization curves as a function of Cr content are plotted in Fig. 9. The alloy containing 7 at% Cr shows a large passive region of 1.13 V, a low passive current density of 2.33×10^{-6} A/cm^2 and a low transpassive potential of 1.25 V. When Cr content exceeds 7 at%, the corrosion behavior changes little with more Cr addition, indicating that a small amount of Cr addition below 7 at% can effectively improve the corrosion resistance of the Fe-based alloy in this study.

In addition, as shown in Fig. 8, the alloys containing more than 3 at % Cr show more than one active dissolution peaks in polarization curves, indicating the formation of the passive film was not completed through one step. It is also noteworthy that abrupt changes of the polarization curves occur when Cr content increases from 3 to 4 at% and from 5 to 7 at%, respectively, indicating the dramatic changes of the overall corrosion performance. There is an obvious passivation region for the polarization curve of the alloy with 4 at% Cr addition, but no passivation region for that with 3 at% Cr addition. The stability of amorphous structure is similar for the alloys with 3 and 4 at% Cr, but the latter has more complete passive film with better protective ability. Therefore, the abrupt polarization behavior changes of alloys when Cr addition increases from 3 to 4 at% can be attributed to the better protection of the complete oxidation film. When Cr addition increases from 5 to 7 at%, the ΔE and ΔE_{tp} go through a large increase, indicating an improvement of the corrosion resistance. The alloys with 5 at% and higher Cr content all have uniform and complete passive films as shown in Fig. 7. Meanwhile, the crystallization process transforms from a three-stage to a two-stage behavior when Cr increases from 5 to 7 at%, indicating the amorphous structure becomes more stable. Moreover, the polarization curves have little change for the alloys with more than 7 at % Cr, which have similar stability of amorphous structure and similar oxide films. As a result, it can be concluded that the improvement of the structural stability when Cr content increases from 5 to 7 at % results in the increase of the corrosion resistance. Based on the above analyses, the abrupt changes are related to the comprehensive effects of the stability of amorphous structure and the protective ability of the oxide film formed on the surface of alloys.

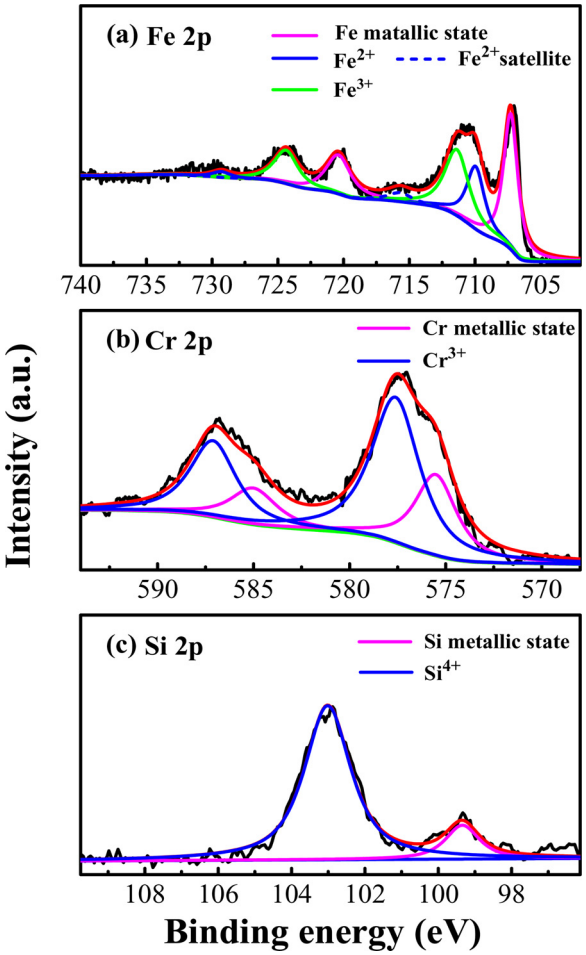

Fig. 10. XPS spectra of (a) Fe 2p, (b) Cr 2p and (c) Si 2p of the $Fe_{72.5}Si_{9.5}B_{11}Cr_7$ amorphous ribbons after electrochemical measurement in 0.1 M NaCl solution.

The studies on potentiodynamic polarization suggest that the corrosion resistance of the FeSiB amorphous alloy is effectively improved by minor Cr addition. Considering the corrosion resistance, soft magnetic properties and materials cost comprehensively, the optimal amount of Cr addition is 5 at%. The alloy with 5 at% Cr exhibits a low coercive force of 2.02 A/m, a saturation magnetization of 1.19 T, a low passive current density of 2.67×10^{-6} A/m and a large ΔE of 0.44 V.

3.3. Chemical characteristics of the surface films

To better understand the effect of Cr addition on the corrosion mechanism, XPS analysis was performed to characterize the chemical composition of oxide films formed on the surfaces of the amorphous ribbons after electrochemical testing. Fig. 10 shows the spectra of Fe 2p, Cr 2p and Si 2p of the alloy with 7 at% Cr after Ar-ion sputtering for 15 s. The spectra of these alloys consist of peaks corresponding to their oxidized states (ox) in the surface film and the metallic states (m) in the underlying alloy surface just beneath the surface film [21,22]. The Fe 2p spectra corresponding to the peaks of Fe $2p^{1/2}$ and $2p^{3/2}$ include the peaks of the metallic state (Fe^m), Fe^{2+} and Fe^{3+} oxidized states (Fe^{ox}). In addition, the Fe^{2+} satellite peak occurs at about 6 eV higher binding

Fig. 11. A schematic diagram of the compositional distribution on the surface of the specimen after electrochemical measurement in 0.1 M NaCl solution.

energies than the main Fe 2p peaks [23]. The Cr 2p peaks represent the metallic state (Cr^{m}) and Cr^{3+} oxide states (Cr^{ox}). From the Si 2p spectrum, Si exists in the forms of metallic state and SiO_2. Based on the XPS analysis, the surface film of the specimen after electrochemical testing consists of Fe^{2+}, Fe^{3+}, Cr^{3+}, Si^{4+} and B^{3+}, while the underlying alloy surface is composed of Fe^{m}, Cr^{m}, Si^{m} and B^{m}, as shown clearly in the schematic diagram of the compositional distribution on the alloy surface, as shown in Fig. 11.

Fig. 12 shows the XPS depth profile spectra for the Fe 2p and Cr 2p of the alloys with 2 and 7 at% Cr after Ar-ion sputtering for 15, 125 and 225 s, respectively. The spectra were normalized to the same height at their maximum peaks for comparison. The peak positions of Fe and Cr in the oxide films are similar to each other although there are some differences between their peak intensities. With increasing the etching time, the peak intensities of the metallic state (Fe^{m} and Cr^{m}) in the Fe 2p and Cr 2p XPS spectra of the alloys increase while the peaks for the oxidized state disappear after Ar-ion sputtering for 125 s, indicating that the oxide layer of the ribbons was removed after etching for 125 s. No peak corresponding to Fe^{ox} or Cr^{ox} exists in the Fe 2p and Cr 2p XPS spectra of the alloys after etching for 225 s.

After integrating intensities of the peaks for individual species, the composition of the surface film and the underlying alloy surface were calculated quantitatively [14,15]. The fractions of the alloying elements in the surface films and the underlying alloy surfaces of $Fe_{79.5-x}Si_{9.5}B_{11}Cr_x$ amorphous ribbons (x = 2, 7) after electrochemical tests compared to their nominal ratios are summarized in Fig. 13. In comparison with the nominal ratio, the fractions of Cr and Si in the surface film and the underlying alloy surface increase while that of Fe decreases after electrochemical test in 0.1 M NaCl solution. Besides, when Cr addition rises from 2 to 7 at%, the fractions of Cr^{ox} and Si^{ox} in the surface film increase while that of Fe^{ox} decreases. The Cr/Fe ratio is defined to represent the enrichment condition of Cr element. Table 3 shows the Cr/Fe ratio for the alloys with 2 and 7 at% Cr in nominal, as well as that in the oxide film, the underlying alloy surface and the alloy after Ar-ion sputtering for 125 and 225 s. As shown in Table 3, the Cr/Fe ratios of the specimen after sputtering are almost the same as their nominal ratios, indicating the oxide films of the alloys have been removed. This result verifies that the composition of the as-spun ribbons does not deviate from their nominal ratios. The Cr/Fe ratios in the surface film and the underlying alloy surface of the alloys with 2 and 7 at% Cr are all higher than their nominal ratios, and the Cr/Fe ratios of the alloys with 7 at% Cr are higher than that of the alloys with 2 at% Cr. Thus, it can be suggested that Cr element is enriched in the oxide film of the Cr-containing alloys. According to the work of Pang et al., the formation of Cr-enriched oxide film is due to the fast dissolution of iron during the initial period in the active state [11]. Obviously, the enrichment of Cr in the oxide film is the main reason that contributes to the effective protection of oxide film and results in high corrosion resistance of the Cr-containing alloys.

The relationship between the high corrosion resistance and the formation of a Cr-rich passive film for the FeSiBCr amorphous system derived from XPS analysis is similar to that for conventional stainless steels [24–26]. However, more than 12.5 at.% Cr is required to significantly increase the corrosion resistance of the stainless steels according to the n/8 principle while even only 5–7 at.% Cr addition can improve the corrosion properties of the FeSiB amorphous alloys dramatically in this study. Several studies on amorphous alloys have also reported that only 4–8 at.% Cr addition could achieve good passivity and enhance their corrosion resistance significantly [7,8,12,27]. In general, compared to stainless steels, amorphous alloys need lower Cr contents to achieve good passivity and high corrosion resistance. The superiority in Cr contents of amorphous alloys may be ascribed to its amorphous structure. Firstly, compared to stainless steels, due to the rapid cooling rate, amorphous alloys are composed of a chemically homogenous single phase without any physical or chemical heterogeneity, forming a more uniform passive film on the amorphous substrate that provides better protection against corrosion. As a result, lower amount of Cr in the passive film could achieve necessary stability than stainless steels [28,29]. Secondly, the metastable nature of the amorphous alloys enables them higher chemical reactivity, which enhances the enrichment of the oxidized Cr element in the film and hastens the formation of a uniform corrosion-resisting passive film. [28]. Due to the rapid formation of the uniform passive film, a smaller amount of Cr enables amorphous alloys to achieve high corrosion resistance than stainless steels. It can be seen that amorphous alloys have great superiority over traditional stainless steels in application where corrosion resistance is important.

4. Conclusions

In this study, the effects of compositional optimization with Cr addition on the thermal stability, soft magnetic properties and corrosion resistance of FeSiB amorphous alloys were systematically investigated. The origin of high corrosion resistance of the Cr-containing alloys was also discussed. This study will be beneficial to explore a new FeSiB amorphous alloy system with high corrosion resistance and thermal stability as well as excellent soft magnetic properties. The results are summarized as follows:

(1) The thermal stability, soft magnetic properties and corrosion resistance of $Fe_{79.5-x}Si_{9.5}B_{11}Cr_x$ (x = 0, 1, 2, 3, 4, 5, 7, 9 and 11 at%) amorphous alloys have been improved with a small amount of Cr addition. The coercivity of the alloys was effectively reduced from 2.46 to 1.47 A/m by the addition of Cr element although the saturation magnetization decreased slightly.

(2) The corrosion resistance of FeSiB alloys was dramatically enhanced with a minor Cr addition due to the formation of the Cr-rich protective films. The corrosion rate of the alloys in 0.1 M NaCl solution decreased from 1.83×10^{-1} to 3.91×10^{-4} mm·year^{-1} as Cr content increased from 0 to 5 at%. The FeSiB alloy with a low passive current density of 2.67×10^{-6} A/cm^2 and a large passive potential region of 0.44 V was obtained by adding 5 at% Cr element. The Cr-containing alloys also exhibited large passive regions

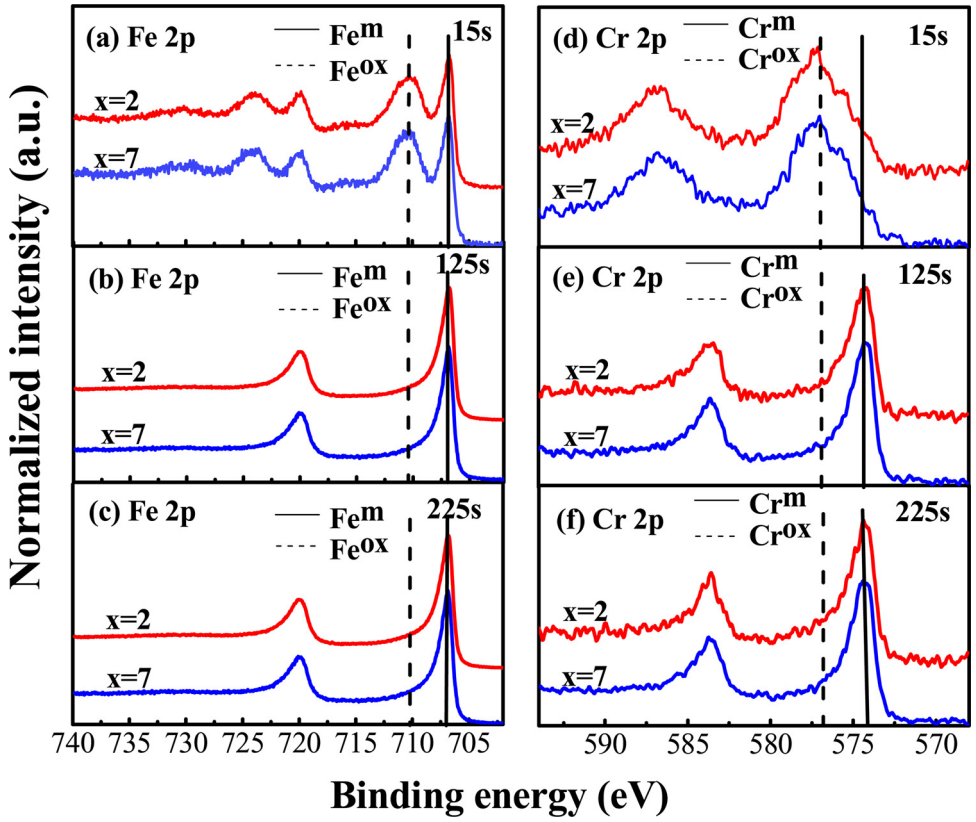

Fig. 12. (a–c) Fe 2p and (d – f) Cr 2p XPS depth profile spectra of x = 2 and x = 7 alloys with Ar – ion sputtering for 15, 125, and 225 s, respectively. (superscript m: metallic state; superscript ox: metal oxide state).

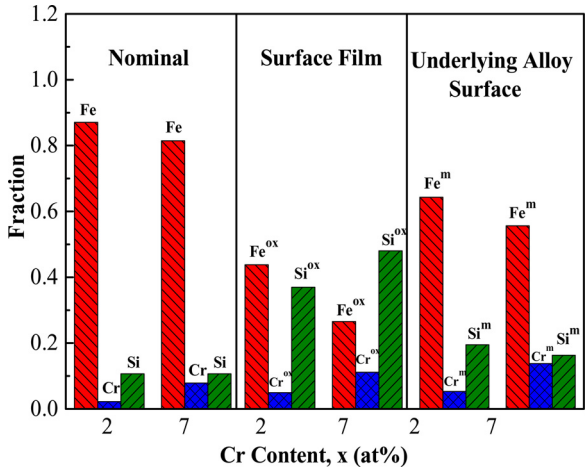

Fig. 13. The fractions of the alloying elements in the surface films and the underlying alloy surfaces of $Fe_{79.5-x}Si_{9.5}B_{11}Cr_x$ amorphous ribbons (x = 2, 7) compared to their nominal ratios.

Table 3
The nominal Cr/Fe ratio and that in the surface films and the underlying alloy surfaces for the alloys with 2 and 7 at% Cr, as well as the Cr/Fe ratios of the alloys after Ar-ion sputtering for 125 (Sput125) and 225 s (Sput225), respectively.

Cr content (at%)	Cr / Fe				
	Nominal ratio	Surface film	Underlying alloy surface	Sput125	Sput225
x = 2	0.0258	0.1131	0.0826	0.0286	0.0298
x = 7	0.0966	0.4204	0.2476	0.1041	0.0914

exceeding 1.13 V when Cr content was higher than 5 at%.

(3) The chemical composition analysis based on XPS showed that the oxide films of specimen after electrochemical tests consisted of Fe^{2+}, Fe^{3+}, Cr^{3+}, Si^{4+} and B^{3+}. As the content of Cr element increased from 2 to 7 at%, the fractions of Cr^{ox} and Si^{ox} in the surface film increased while the Fe^{ox} decreased obviously, which was also confirmed from the formation of a homogeneous passive film covering on the alloy surface as observed by SEM, leading to the enhancement of corrosion resistance of FeSiBCr amorphous alloys.

(4) The quantitative analysis of XPS spectra revealed that the Cr element was enriched in the oxide film of the Cr-containing amorphous alloy. Besides, it was also found that the Cr/Fe ratios in the surface film and the underlying alloy surface of the alloys with Cr addition were all higher than their nominal ratios, which is the reason for protection improvement of oxide film in Cr-containing alloys.

Acknowledgements

This work was supported by the National Natural Science Foundation of China (Grant Nos. 51631003, 51601038 and 51501037), the State Key Development Program for Basic Research of China (Grant No. 2016YFB0300502), the Natural Science Foundation of Jiangsu Province, China (Grant No. BK20171354), the Fundamental Research Funds for the Central Universities (Grant No. 2242017K40189) and Jiangsu key laboratory for advanced metallic materials (Grant No. BM2007204).

References

[1] F.E. Luborsky, J.J. Becker, J.L. Walter, H.H. Liebermann, Formation and magnetic properties of Fe-B-Si amorphous alloys, IEEE Trans. Magn. 15 (1979) 1146–1149.
[2] R. Hasegawa, Amorphous magnetic materials-a history, J. Magn. Magn. Mater. 100

(1991) 1–12.
[3] D. Szewieczek, A. Baron, Electrochemical corrosion properties of amorphous $Fe_{78}Si_{13}B_9$ alloy, J. Mater. Process. Technol. 157 (2004) 442–445.
[4] Y.J. Li, B. An, Y.G. Wang, Y. Liu, H.D. Zhang, X.G. Yang, W.M. Wang, Severe corrosion behavior of $Fe_{78}Si_9B_{13}$ glassy alloy under magnetic field, J. Non-Cryst. Solids 392–393 (2014) 51–58.
[5] B. An, Y.J. Li, Y. Liu, Y.G. Wang, L.C. Zhang, W.M. Wang, Unique corrosion behavior of $Fe_{78}Si_9B_{13}$ glassy alloy with different circumferential speeds under various chloride ion levels, J. Alloys Compd. 593 (2014) 16–23.
[6] L.L. Meng, X.Y. Li, J. Pang, L. Wang, B. An, L.J. Yin, K.K. Song, W.M. Wang, Casting atmosphere effects on the precipitations, magnetism, and corrosion resistance of $Fe_{78}Si_9B_{13}$ glassy alloys, Metall. Mater. Trans. 44 (2013) 5122–5133.
[7] M. Naka, K. Hashimoto, T. Masumoto, High corrosion resistance of chromium-bearing amorphous iron alloys in neutral and acidic solutions containing chloride, Corrosion 32 (1976) 146–152.
[8] S.J. Pang, T. Zhang, K. Asami, A. Inoue, Effects of chromium on the glass formation and corrosion behavior of bulk glassy Fe-Cr-Mo-C-B alloys, Mater. Trans. 43 (2002) 2137–2142.
[9] X. Li, C.T. Chang, T. Kubota, C.L. Qin, A. Makino, A. Inoue, Effect of Cr addition on the glass-forming ability, magnetic, mechanical and corrosion properties of $(Fe0.76Si_{0.096}B_{0.096}P_{0.048})_{100-x}Cr_x$ bulk glassy alloys, Mater. Trans. 49 (2008) 2887–2890.
[10] Y.J. Huang, Y.Z. Guo, H.B. Fan, J. Shen, Synthesis of Fe-Cr-Mo-C-B amorphous coating with high corrosion resistance, Mater. Lett. 89 (2012) 229–232.
[11] S.J. Pang, T. Zhang, K. Asami, A. Inoue, Bulk glassy Fe-Cr-Mo-C-B alloys with high corrosion resistance, Corros. Sci. 44 (2002) 1847–1856.
[12] B.L. Shen, M. Akiba, A. Inoue, Effect of Cr addition on the glass-forming ability, magnetic properties and corrosion resistance in FeMoGaPCBSi bulk glassy alloys, J. Appl. Phys. 100 (2006) 043523.
[13] K. Inomata, M. Hasegawa, S. Shimanuki, Magnetic properties of amorphous Fe-Cr-Si-B alloys, IEEE Trans. Magn. 17 (1981) 3076–3078.
[14] K. Asami, K. Hashimoto, S. Shimodaira, XPS determination of compositions of alloy surfaces and surface oxides on mechanically polished iron-chromium alloys, Corros. Sci. 17 (1977) 713–723.
[15] K. Asami, K. Hashimoto, An XPS study of the surfaces on Fe-Cr, Fe-Co and Fe-Ni alloys after mechanical polishing, Corros. Sci. 24 (1984) 83–97.
[16] K. Asami, A precisely consistent energy calibration method for X-ray photoelectron spectroscopy, J. Electron. Spectrosc. Relat. Phenom. 9 (1976) 469–478.
[17] K. Asami, K. Hashimoto, The x-ray photo-electron spectra of several oxides of iron and chromium, Corros. Sci. 17 (1977) 559–570.
[18] A. Inoue, B.L. Shen, Soft magnetic bulk glassy Fe-B-Si-Nb alloys with high saturation magnetization above 1.5 T, Mater. Trans. 43 (2002) 766–769.
[19] T. Bitoh, A. Makino, A. Inoue, Magnetization process and coercivity of Fe-(Al, Ga)-(P, C, B, Si) soft magnetic glassy alloys, Mater. Trans., JIM 45 (2004) 1219–1227.
[20] T. Bitoh, A. Makino, A. Inoue, Origin of low coercivity of $(Fe0.75B_{0.15}Si_{0.10})_{100-x}Nb_x$ (x = 1–4) glassy alloys, J. Appl. Phys. 99 (2006) 08F102.
[21] C.L. Qin, Y.Q. Zeng, D.V. Louzguine, N. Nishiyama, A. Inoue, Corrosion resistance and XPS studies of Ni-rich Ni-Pd-P-B bulk glassy alloys, J. Alloys Compd. 504 (2010) S172–S175.
[22] C.L. Qin, J.J. Oak, N. Ohtsu, K. Asami, A. Inoue, XPS study on the surface films of a newly designed Ni-free Ti-based bulk metallic glass, Acta Mater. 55 (2007) 2057–2063.
[23] T. Yamashita, P. Hayes, Analysis of XPS spectra of Fe^{2+} and Fe^{3+} ions in oxide materials, Appl. Surf. Sci. 254 (2008) 2441–2449.
[24] R. Kirchheim, B. Heine, H. Fischmeister, S. Hofmann, H. Knote, U. Stolz, The passivity of iron-chromium alloys, Corros. Sci. 29 (1989) 899–917.
[25] M.D. Archer, C.C. Corke, B.H. Harji, The electrochemical properties of metallic glasses, Electrochim. Acta 32 (1987) 13–26.
[26] M. Madinehei, P. Bruna, M.J. Duarte, E. Pineda, J. Klemm, F.U. Renner, Glass-formation and corrosion properties of Fe-Cr-Mo-C-B glassy ribbons with Cr content, J. Alloy Compd. 615 (2014) S128–S131.
[27] Z.L. Long, Y. Shao, X.H. Deng, Z.C. Zhang, Y. Jiang, P. Zhang, B.L. Shen, A. Inoue, Cr effects on magnetic and corrosion properties of Fe-Co-Si-B-Nb-Cr bulk glassy alloys with high glass-forming ability, Intermetallics 15 (2007) 1453–1458.
[28] K. Hashimoto, What we have learned from studies on chemical properties of amorphous alloys? Appl. Surf. Sci. 257 (2011) 8141–8150.
[29] C.A.C. Souza, D.V. Ribeiro, C.S. Kiminami, Corrosion resistance of Fe-Cr-based amorphous alloys: an overview, J. Non-Cryst. Solids 442 (2016) 56–66.